GPS-SNR-based detection of severe weather events: two case studies of summer 2021 in Switzerland

Matthias Aichinger-Rosenberger[1], Martin Aregger[2], Jerome Kopp[2], and Benedikt Soja[1]

[1]Institute of Geodesy and Photogrammetry, ETH Zurich
[2]University of Bern

July 8, 2023

Abstract

Global Navigation Satellite Systems (GNSS) have become a valuable tool for remote sensing, as signals can be used for monitoring soil and snow properties as well as water vapor in the atmosphere. By using L-band carrier frequencies, GNSS acts as an all-weather-operation system. Nevertheless, severe weather can still have an impact on the strength of signals received at a ground station, as we show in this study. We investigate Signal-to-Noise Ratio (SNR) from the Global Positioning System (GPS) during two thunderstorm events, which produced excessive amounts of rain and hail. We make use of a GPS-SNR-based algorithm, developed for the detection of hail particles from volcanic eruptions. Results indicate that the investigated thunderstorm events are visible in SNR observations. Affected satellites show a significant SNR drop during event periods, which are determined by weather radar observations. Thus, results suggest the possibility of detecting severe weather systems using GNSS-SNR observations.

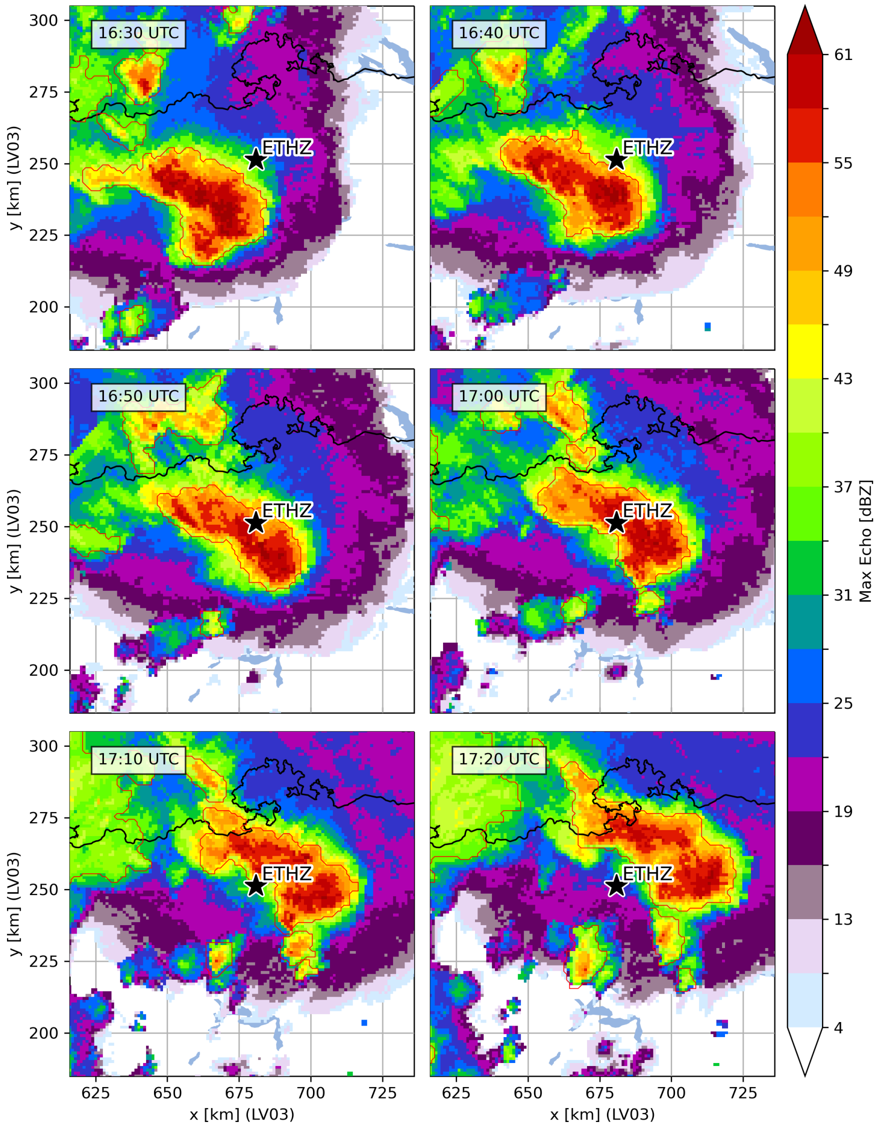
16:30 UTC
16:40 UTC
16:50 UTC
17:00 UTC
17:10 UTC
17:20 UTC
ETHZ
y [km] (LV03)
x [km] (LV03)
Max Echo [dBZ]
300
275
250
225
200
625
650
675
700
725
61
55
49
43
37
31
25
19
13
4

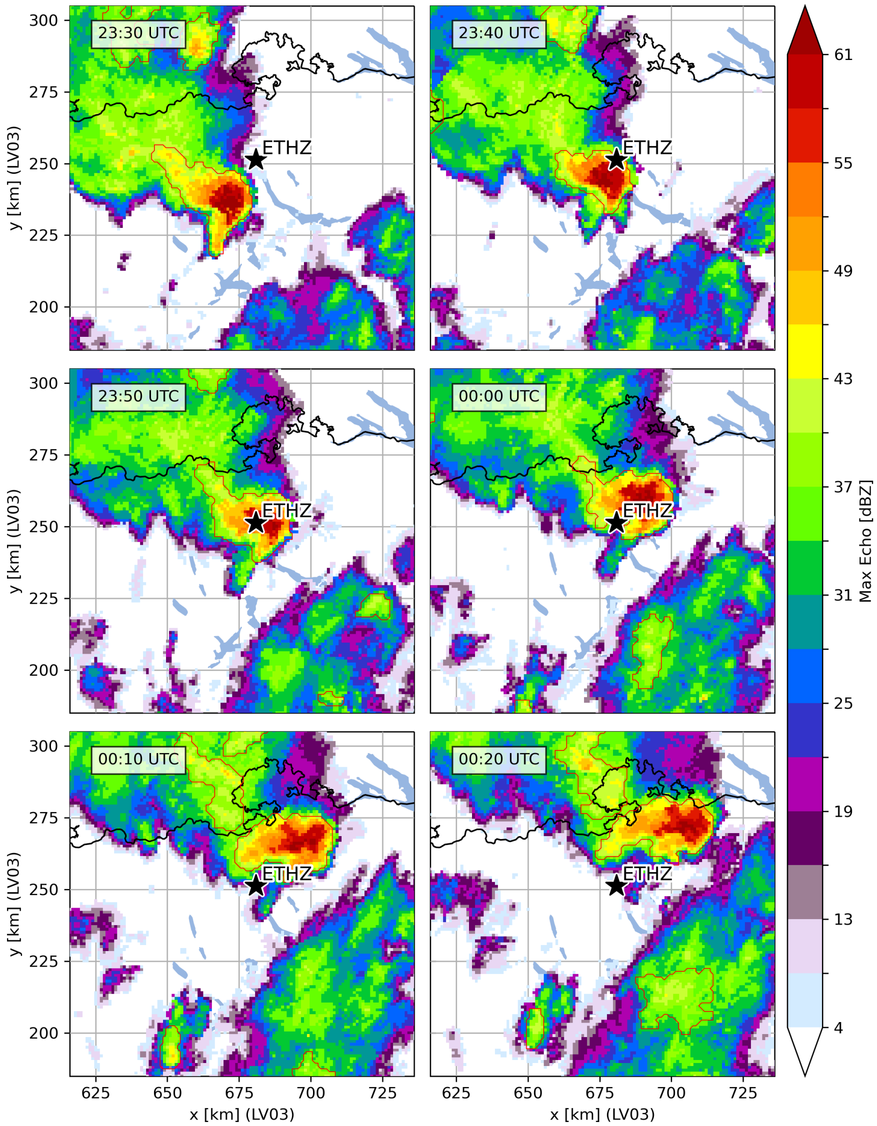
23:30 UTC
23:40 UTC
23:50 UTC
00:00 UTC
00:10 UTC
00:20 UTC
ETHZ
y [km] (LV03)
x [km] (LV03)
Max Echo [dBZ]
4
13
19
25
31
37
43
49
55
61

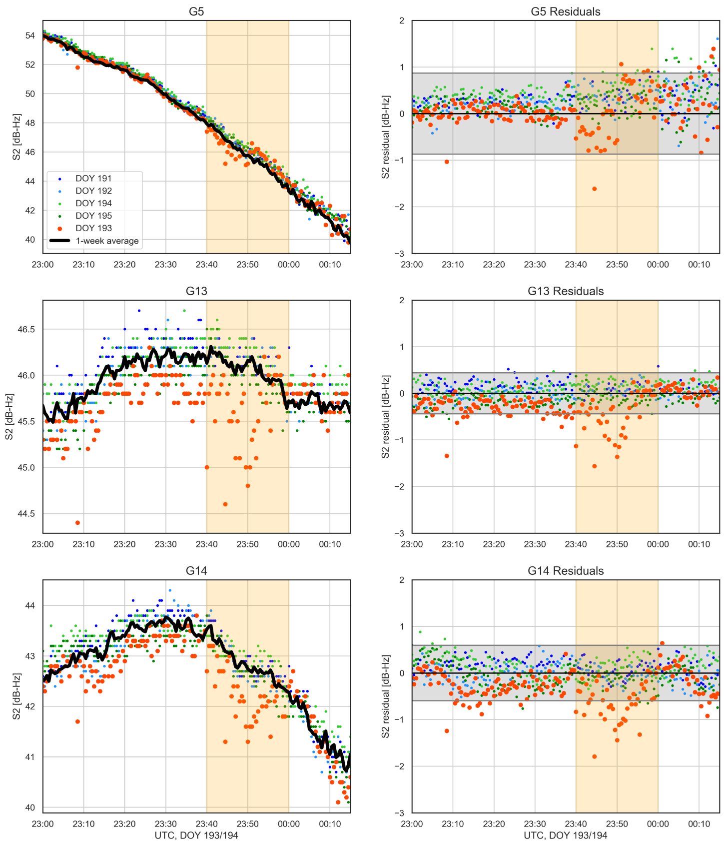
G5
G5 Residuals
G13
G13 Residuals
G14
G14 Residuals
S2 [dB-Hz]
S2 residual [dB-Hz]
DOY 191
DOY 192
DOY 194
DOY 195
DOY 193
1-week average
UTC, DOY 193/194

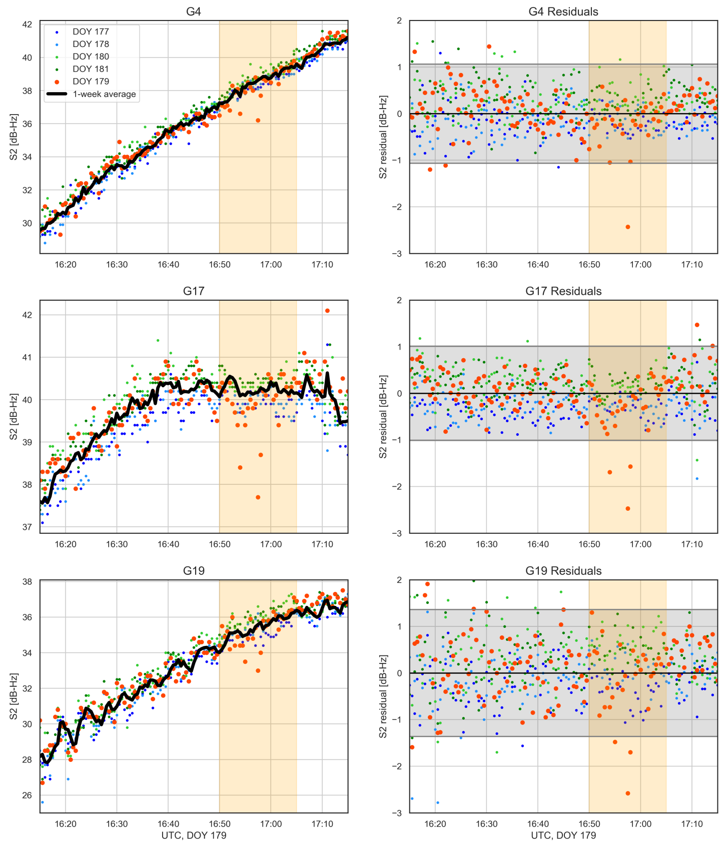
G4
DOY 177
DOY 178
DOY 180
DOY 181
DOY 179
1-week average
S2 [dB-Hz]
G4 Residuals
S2 residual [dB-Hz]
G17
S2 [dB-Hz]
G17 Residuals
S2 residual [dB-Hz]
G19
S2 [dB-Hz]
UTC, DOY 179
G19 Residuals
S2 residual [dB-Hz]
UTC, DOY 179

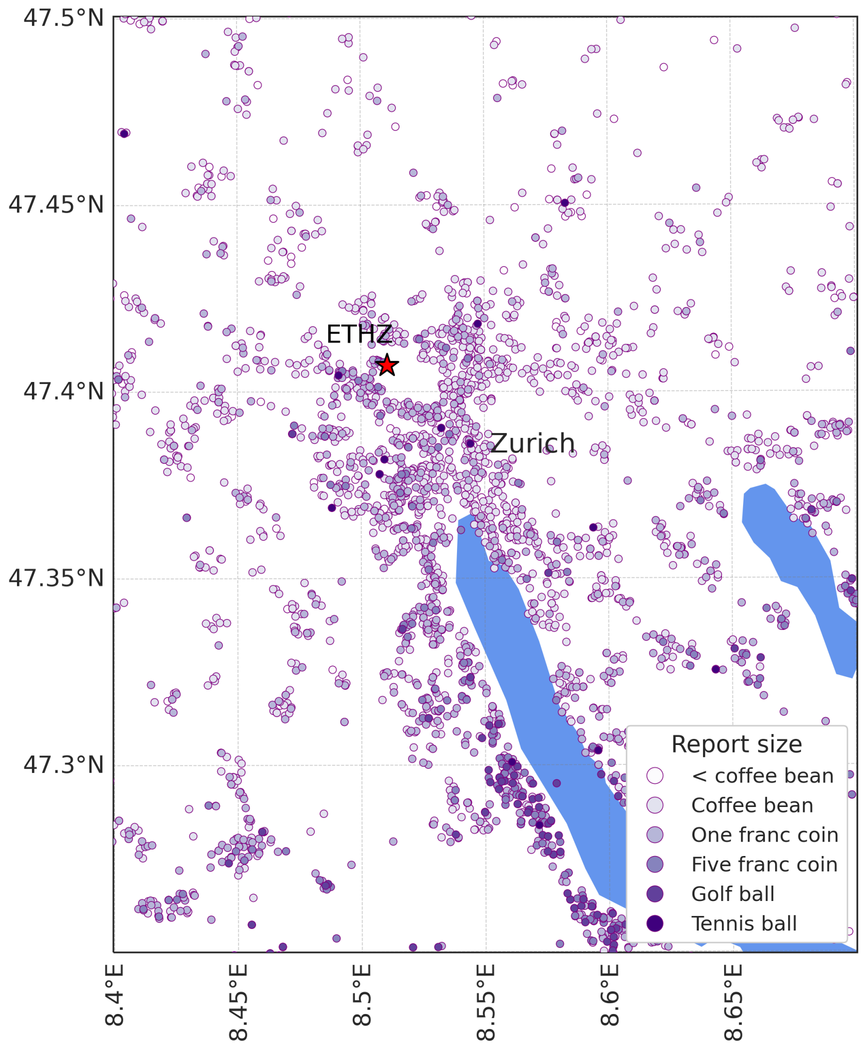
47.5°N
47.45°N
47.4°N
47.35°N
47.3°N
8.4°E
8.45°E
8.5°E
8.55°E
8.6°E
8.65°E
ETHZ
Zurich
Report size
< coffee bean
Coffee bean
One franc coin
Five franc coin
Golf ball
Tennis ball

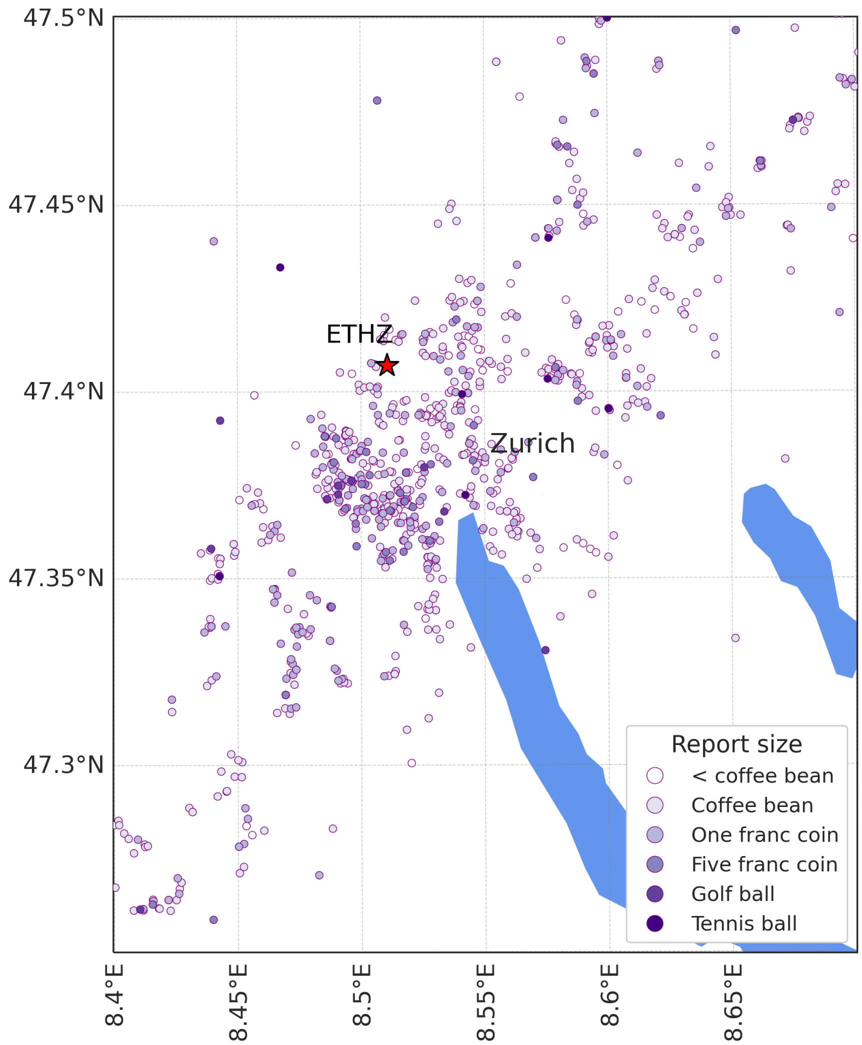

47.5°N
47.45°N
47.4°N
47.35°N
47.3°N
8.4°E
8.45°E
8.5°E
8.55°E
8.6°E
8.65°E
ETHZ
Zurich
Report size
< coffee bean
Coffee bean
One franc coin
Five franc coin
Golf ball
Tennis ball

GPS-SNR-based detection of severe weather events: two case studies of summer 2021 in Switzerland

Matthias Aichinger-Rosenberger[1,2], Martin Aregger[3,4], Jerome Kopp[3,4], Benedikt Soja[1]

[1]Institute of Geodesy and Photogrammetry, ETH Zurich, Zurich, Switzerland
[2]Current address: Constellation Observing System for Meteorology Ionosphere and Climate (COSMIC) Program , University Corporation for Atmospheric Research (UCAR), Boulder, Colorado, USA
[3]Institute of Geography, University of Bern, Bern, Switzerland
[4]Oeschger Center for Climate Change Research, University of Bern, Bern, Switzerland

Key Points:

- GNSS
- Severe weather detection
- Signal-to-Noise ratio

Corresponding author: Matthias Aichinger-Rosenberger, `maichinger@ethz.ch`

Abstract

Global Navigation Satellite Systems (GNSS) are not only a state-of-the-art sensor for positioning and navigation applications but also a valuable tool for remote sensing of the environment. GNSS signals can be used for monitoring soil and snow properties as well as water vapor contained in the atmosphere at high temporal resolution. Through the usage of L-band carrier frequencies, GNSS acts as an all-weather-operation system, which offers substantial benefits compared to, e.g., optical remote sensing systems. Nevertheless, severe weather events can still have a significant impact on the strength of signals received at a ground station, as we show in this study. We investigate Signal-to-Noise Ratio (SNR) observations from the Global Positioning System (GPS) during two severe thunderstorm events, which produced excessive amounts of rain and hail over the city of Zurich, Switzerland. Therefore, we make use of a GPS-SNR-based algorithm originally developed for the detection of hail particles from volcanic eruption events. Results indicate that, although GNSS observations are considered to be fairly insensitive to the presence of hydrometeors, the investigated thunderstorm events are visible in SNR observations. SNR levels of affected satellites show a significant drop during event periods, which are determined by weather radar observations. Thus, these results suggest the possibility of detecting severe weather systems by utilization of GNSS-SNR observations.

Plain Language Summary

Over the last two decades, observations from Global Navigation Satellite Systems (GNSS) have proven to be a useful data source for meteorology. Typically, signal delays introduced by the presence of water vapor along the signal path are utilized for analysing and predicting the atmospheric moisture field, and subsequently, precipitation. However, other GNSS observations types can also be influenced by severe thunder- and hailstorms, which are high-impact weather events. In this study, we show that is the case for the Signal-to-Noise Ratio (SNR) of GNSS signals. We investigate two large thunderstorm events which took place over the city of Zurich. These events are visible as significant degradation in SNR data of GNSS satellites. By analysing radar images we are able to show that the time period of SNR degradation closely corresponds to the period of strongest precipitation intensity observed by radar. Although more detailed investigations have to be carried out in the future, these initial findings indicate the potential of GNSS-SNR data for observation of severe weather events and strengthen the status of GNSS as a valuable tool for meteorological applications.

1 Introduction

Extreme weather events, such as severe thunderstorms and associated natural hazards, represent a significant risk to human life and property through lightning, heavy precipitation, hail and strong winds. These phenomena are very localized in space and can develop within timescales ranging from tens of minutes to a few hours, making them difficult to forecast precisely using numerical weather prediction (NWP) models. As most climate projections indicate an increasing frequency of such events in most regions (Rädler et al., 2019; Ridder et al., 2022), accurate forecasts and observational methods as well as the development of early-warning and resilience systems become increasingly important.

Over the last two decades, Global Navigation Satellite Systems (GNSS) have been established as a state-of-the-art observation system for navigation and monitoring purposes. In atmospheric sciences, troposphere products from GNSS are recognized as valuable data sources for NWP and climate monitoring. The presence of atmospheric water vapor affects signal propagation by causing a delay in GNSS signals, which can be determined alongside the receiver coordinates and clock error. This technique, commonly referred to as GNSS Meteorology (Bevis et al., 1992), has been used extensively for data assimilation systems at almost all major NWP centers worldwide and its benefits have been shown by a large number of studies (see Guerova et al. (2016) or Jones et al. (2020) for a good overview). Over the last years, an increasing number of authors have focused on signatures of severe weather events, such as extreme precipitation (e.g. Wilgan et al. (2023), Arief and Heki (2020)).

In contrast to GNSS Meteorology, which requires a comprehensive GNSS processing approach to determine tropospheric signal delays, other techniques have been established that make use of raw GNSS observations. One example is GNSS Reflectometry (GNSS-R), a technique that aims to infer information about the surface from which a reflected signal travels to the receiver. This way, quantities such as soil moisture (K. Larson et al. (2008)) or snow depth (K. Larson et al. (2009)) can be retrieved. Furthermore, space-borne GNSS-R retrievals are able to sense precipitation over the ocean by quantifying the rain attenuation impact on GNSS-R wind speed products (Asgarimehr et al., 2018, 2019). For ground-based GNSS-R, the basic observation type is the Signal-to-Noise Ratio (SNR) of GNSS signals (GNSS-SNR). In GNSS processing, SNR often only represents an indication of data quality and the level of multipath interference. Besides this, it is still rarely used in GNSS data analysis. In addition to the impact of surface properties on GNSS-SNR, there are also processes which can affect the SNR of direct signals. One example is volcanic eruptions, which have been studied using GNSS observations by a number of authors over the last decades (e.g. Shimada et al. (1990); Lee et al. (2015); Grapenthin et al. (2022)). Most of these studies used GNSS observations to monitor ground deformation near erupting volcanoes, but not to detect effects of the eruption above ground, e.g., the evolution of the plume. Modelling of volcanic plumes was first shown by Houlié et al. (2005a) for the eruption of Miyakejima volcano (Japan) and Mount St.Helens (Houlié et al., 2005b) and this approach was developed further by Grapenthin et al. (2013). Most recently, Cegla et al. (2022) investigated the 2014 Sakurajima Eruption, by a comparison of Zenith Total Delays (ZTDs) from GNSS and ray-tracing methods.

All of those studies treated the effects of the plume on signal propagation as an unmodeled atmospheric error, originating from the presence of a large amount of sand and ash particles. This idea is reasonable, since sand and ash particles affect signal propagation in a similar way as gaseous atmospheric constituents, although the magnitude of this effect is smaller. This was shown by Solheim et al. (1999) in a theoretical investigation carried out over two decades ago. They also found that under standard atmospheric conditions, GNSS measurements experience no significant impact from hydrometeors (small amounts of water or ice particles) present along the signal path. However, they also note that this might change for severe weather events, where both the amount and size of hydrometeors are much more substantial. As for volcanic particles, the effect of hydrometeors on GNSS products during severe weather conditions was primarily studied using troposphere products, such as ZTD or Slant Total Delays (STDs). Studies such as Brenot et al. (2006), Douša et al. (2016) or Hordyniec et al. (2018) found significant effects under extreme weather conditions, accounting for a mismodeling of, e.g., ZTD of up to cm-level. However, one major disadvantage of investigating hydrometeors as a tropospheric mismodeling is the fact that comprehensive GNSS processing is necessary to derive all products to be analysed. In order to avoid this, K. M. Larson (2013) introduced a new method for plume detection that is solely based on SNR observations. The study showed the strengths and limitations of the method by presenting results from the 2008 and 2009 eruptions of the Okmok and Mt. Redoubt volcanoes. Plume detections based on GNSS-SNR observations were found to be consistent with independently collected seismic and radar data of the eruptions. In a later study on the 2011 eruption of Grímsvötn Volcano in Iceland, Grapenthin et al. (2018) applied a method that combined SNR and phase residuals to detect volcanic hail.

Our study applies a similar SNR-based detection algorithm as shown in K. M. Larson (2013) on data collected during two severe weather events, which affected the city of Zurich in Switzerland in early summer 2021. Using observations from a nearby GNSS station, we show how hydrometeors affect GNSS-SNR and thus allow for the detection of severe weather events. To our knowledge, this study represents the first investigation on the detection of severe weather events using GNSS-SNR data.

2 Data and methods

2.1 GNSS-SNR

SNR is a raw observation type which is typically recorded by all GNSS receivers and serves as a measure of received signal strength. GNSS-SNR levels depend on both satellite elevation and the actual carrier frequency on which observations are recorded. They increase with satellite elevation, peaking at levels between 50-60 dB-Hz for satellites observed near the zenith direction (90°). Due to the repeatability of GNSS satellite tracks (e.g., with a revolution time of 11 hours and 58 minutes for GPS satellites), satellites cover the same elevation ranges (and therefore comparable SNR levels) for approximately the same time periods on consecutive days. We will make use of this fact in our analysis and the formulation of the detection algorithm introduced in Section 2.4. Following K. M. Larson (2013), we use solely GPS L2C SNR data (in the following termed S2) in this study because of its smaller amount of high-frequency noise at higher elevations compared to L1.

For this study, we utilize GPS-SNR observations from the ETHZ GNSS station collected at a data rate of 30 seconds, available in Receiver Independent Exchange Format (RINEX) 2.11 (Gurtner & Estey, 2007). The station is located in the city of Zurich at the ETH Campus Hoenggerberg and belongs to the Automated GNSS Network of Switzerland (AGNES), operated by the Federal Office of Topography (swisstopo).

2.2 Radar

As a state-of-the-art observing technique for precipitation, weather radar images are the first choice to accurately determine the thunderstorm event time at the respective GNSS sites. Therefore, we make use of operational radar products, stemming from the Swiss weather radar network (Rad4Alp). The network consists of five polarimetric C-band radars at altitudes ranging from 928 m to 2937 m above sea level, operated by MeteoSwiss (Germann et al., 2022). The radars are arranged in a configuration which provides overlapping coverage, ensuring good visibility in the Alps. Here, we use a two-dimensional Cartesian maximum reflectivity composite with a spatial resolution of 1 km x 1 km which is produced every 5 minutes and spans an area of 640 x 710 km^2. For the composite, the polar horizontal reflectivity data from each of the five radars is interpolated into a three-dimensional Cartesian grid on which a column maximum is applied to reduce it to a two-dimensional dataset. High values of reflectivity can be used as an indicator for the presence of intense precipitation and hail (Waldvogel et al., 1979; Germann et al., 2009). To identify individual convective cells and their movements, the reflectivity-based Thunderstorm Radar Tracking (TRT) algorithm is used (Hering et al., 2004).

2.3 Hail crowdsourced reports

Alongside heavy precipitation, severe storms also produce hail. While radar-based hail algorithms exist to estimate the probability of hail on the ground (POH, Waldvogel et al. (1979)) and the maximum expected severe hailstone size (MESHS, Foote et al. (2005)), they are proxy-based and not surface observations. Therefore, we use the crowdsourcing function of the MeteoSwiss app to assess the presence of hail on the ground. The function allows users to report the hail size category, time and location using their smartphone. The reports are previously submitted to plausibility filters to reduce the number of false alarms (Barras et al., 2019).

2.4 Detection algorithm

As mentioned in the introduction, this study makes use of a largely similar plume-detection algorithm as proposed in K. M. Larson (2013). The exact algorithm applied in this study consists of the following steps:

1. Extract GPS-S2 time series from RINEX observation files using the rnx2snr module of the GNSS-IR software gnssrefl (Roesler & Larson, 2018).
2. Filter out all data with elevation angles $< 20°$, which is more likely to be affected by multipath effects
3. Select satellites that are continuously observed during event time as well as 15-30 min before and after.
4. For each satellite:
   (a) Shift the obtained SNR time series by 4 min/day (with respect to the event day) to account for the repetition time of GPS satellite geometry (23h 56min)
   (b) Average time series for ten prior non-event days to build up the background model (i.e., average SNR evolution for the respective elevation range)
   (c) Obtain SNR residuals for the event day by subtracting the background model from the actual SNR observations
   (d) Calculate the mean and standard deviation of SNR residuals (σ_{res}) from all ten non-event days.
   (e) Set the residual mean $\pm 2.5 \cdot \sigma_{res}$ as the nominal level to be used for event detection.

3 Thunderstorm case studies

The month of July 2021 was characterized by a persistent flow bringing moist and unstable air over Switzerland. Thunderstorms occurred regularly with heavy rainfall, hail and strong wind gusts that caused a fair amount of damage (MeteoSwiss (2021a), Kopp et al. (2022)). In the following, we give a short description of two case studies (CS) carried out for thunderstorm events which affected the city of Zurich in early summer 2021, and present results for the application of the detection algorithm outlined in Section 2.4.

3.1 CS1: 28.06.2021

On 28.06.2021, several supercell storms originated in Western Switzerland around 14:00 UTC and then moved along the northern flank of the Swiss Alps following southwest to northeast tracks. Some of these supercells merged and evolved in an intense mesoscale convective system which produced the second largest hail event in Switzerland since 2002 (MeteoSwiss, 2021b), and hailstones of up to 9 cm diameter in central Switzerland, southwest of Zurich (Kopp et al., 2022). This mesoscale convective system approached the city of Zurich and the ETHZ GNSS station from the southwest around 16:40 UTC (Figure 1). Extended areas with maximum radar reflectivity (MAXRE) values of up to 60 dBZ were registered (Figure 1a) as well as the largest daily number of hail crowdsourced reports (Figure 1b).

For CS1, the detection algorithm was applied on observations of satellites G4, G17 and G19. The only selection criteria for these satellites was their continuous tracking over the period of interest (16:15 - 17:15 UTC). Results are presented in Figure 2. The left panel of the figure shows the respective time series of GPS-SNR observations from the event day as well as two days prior and after the event day. The right panel shows the results of the detection algorithm with colored points representing SNR residuals for the same days as shown on the left side. During this period, all three satellites show degraded SNR levels compared to the background model, with the largest degradation corresponding to the largest reflectivity values over the station. The same pattern is also captured

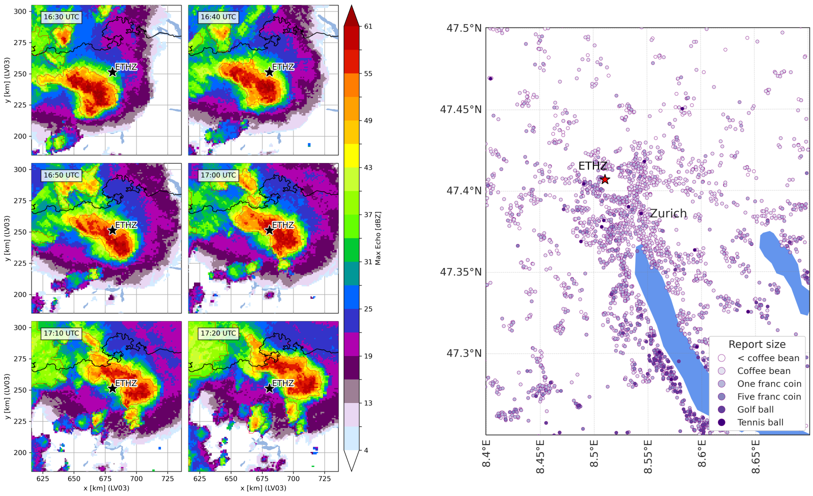

(a) (b)

Figure 1: Radar and crowdsourced hail observations for CS1, 28.06.2021: (a): Images of MAXRE (dBZ) for the region surrounding the ETH Zurich station. Shown are images in five minute intervals. (b): Hail observations for the region surrounding the ETH Zurich station: location of crowdsourced reports (purple dots, largest sizes are darker), location of the ETHZ GNSS station (red star).

by the SNR residuals. Although the number of impacted observations is limited (1-3) for each satellite, their degradation level is significant (2-3 db-Hz), capturing a clear impact of the thunderstorm for the event day. In terms of detection performance, the algorithm does reasonably well, although some detections on non-event days are visible for G17 and G19. There are also a few event detections ahead of the actual event time for satellites G4 and G19. Nevertheless, the largest degradations occur exactly during the period of most intense precipitation, giving a strong indication of the thunderstorm's impact on SNR levels.

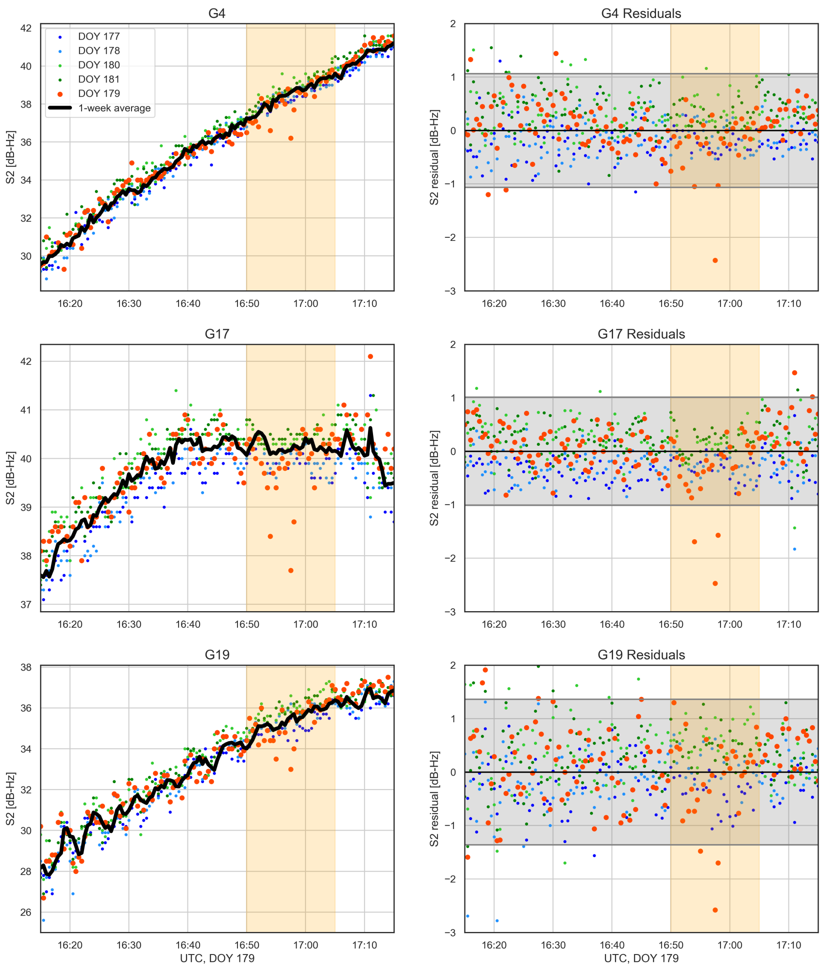

Figure 2: Left panel: SNR observations of satellites G4, G17 and G19 at ETHZ for CS1. Shown are observations from the event day (red, DOY 179), two days prior (blue colors, DOY 177/178) and two days after (green colors, DOY 180/181). In addition, a one-week average over the last ten days prior to the event is shown as the black solid line. Right panel: SNR residuals with respect to the ten-day average for the respective satellite. The nominal detection level is shown as the horizontal gray area. The exact event period determined by radar is color-coded in orange.

3.2 CS2: 12.-13.07.2021

The second storm case investigated in this study took place during the night of 12-13.07.2021, when a supercell thunderstorm crossed Switzerland from France, ahead of an active cold front coming from the west. The storm was particularly intense when it approached the city of Zurich and the ETHZ station from the southwest on 12.07.2021, around 23:40 UTC, with MAXRE values of up to 50 dBZ (Figure 3a). The southwest to northeast movement is clearly visible on the successive MAXRE scans of Figure 3a, with peak reflectivity values lasting for about 20 minutes over the ETHZ station, until approximately 00:00 UTC. The storm also brought hail as shown by the multiple crowdsourced reports sent by the population (Figure 3b). Similar to CS1, the left panel of Fig-

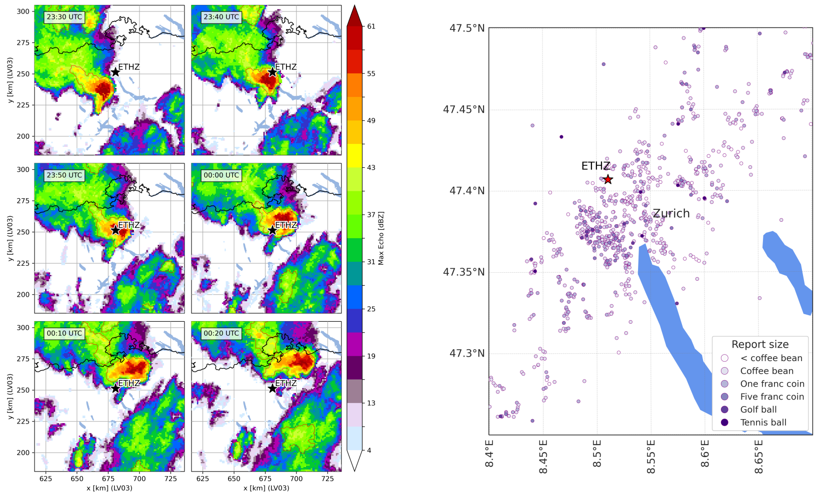

(a) (b)

Figure 3: Radar and crowdsourced hail observations for CS2, 12-13.07.2021: (a): Images of MAXRE (dBZ) for the region surrounding the ETH Zurich stations. Shown are images in five minute intervals. (b): Hail observations for the region surrounding the ETH Zurich stations on 12-13.07.2021: location of crowdsourced reports (purple dots, largest sizes are darker), location of the ETHZ GNSS station (red star).

ure 4 shows the observed SNR time series of CS2 for satellites G05, G13 and G14, continuously observed during the period of interest (23:00-00:00 UTC). Results show a similar pattern as observed for CS1, i.e. a clear degradation in SNR level for all satellites during the period of most intense precipitation (23:40-00:00 UTC) over the ETHZ station. Apart from event time, the observed values agree well with the background model and the noise level is similar throughout the five days shown. This further strengthens the evidence of a distinctive thunderstorm impact on the SNR level, with similar characteristics to CS1. The SNR residuals, shown on the right panel of Figure 4, indicate an even stronger impact of this thunderstorm event on SNR at ETHZ. Some false detections prior and after the event, as well as on other days are again visible, but to a much lesser extent than in CS1. In comparison to CS1, the residual levels are slightly lower (mostly 1-2 db-Hz) but the number of observations affected by the thunderstorm is much higher. For instance, satellites G13 and G14 show a much larger amount of detected events for the event period than any satellite analyzed for CS1. While only one event was detected for G5, several residuals are close to the detection level, still indicating sustained degradation compared to average SNR levels.

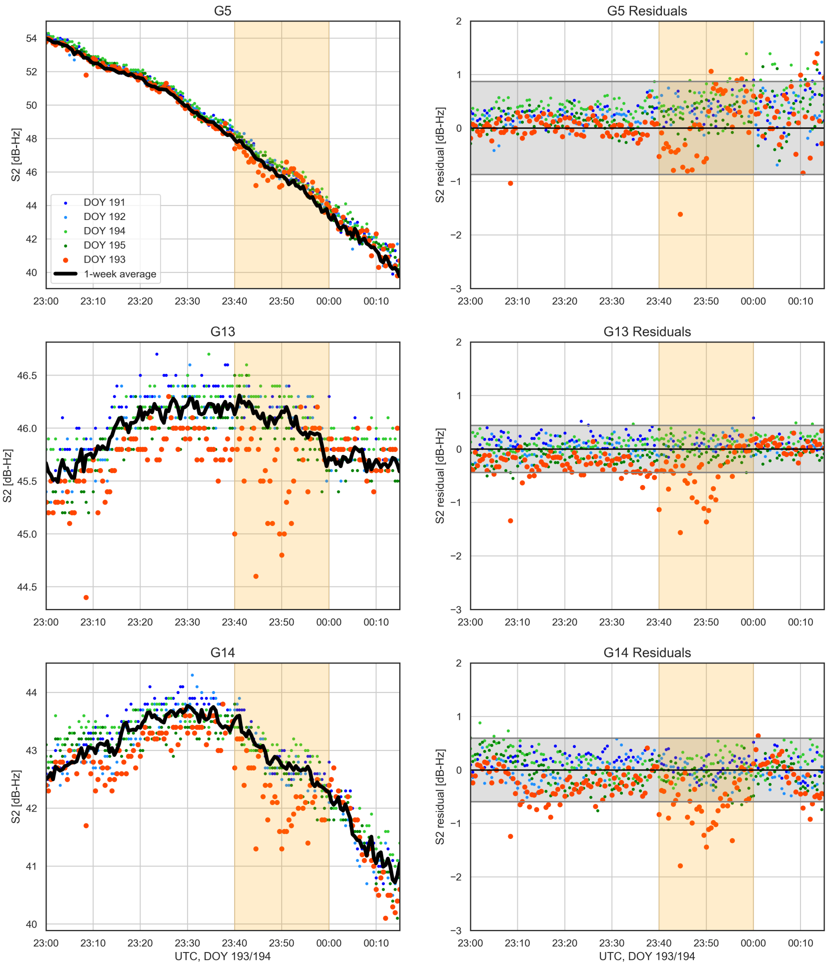

Figure 4: Left panel: SNR observations of satellites G05, G13 and G14 from ETHZ station for time period 12.07.2021 23:00-00:00 UTC. Shown are observations from the event day (red, DOY 193), two days prior (blue colors, DOY 191/192) and two days after (green colors, DOY 194/195). In addition, a one-week average over the last seven days prior to the event is shown as the black solid line. Right panel: SNR residuals with respect to the 10-day average for the respective satellite. The nominal detection level is shown as the horizontal gray area. The exact event period determined by radar is color-coded in orange.

4 Discussion and conclusions

We presented a first investigation on the use of GPS-SNR data for detecting severe thunderstorms by discussing two case studies affecting the ETHZ GNSS station on 28.06.2021 and 12.-13.07 2021. Both cases were accompanied by heavy precipitation and hail, as reported by radar images and crowdsourced hail observations. Our results show a clear SNR degradation during the exact event time at ETHZ, which has been determined from the radar images. Although the number of affected observations is quite small, most of these observations show a significant degradation (~ 2 dB-Hz) compared to average values. These results confirmed both the impact of a severe thunderstorm event on GPS-SNR observations and the capability of the proposed algorithm for detecting such events.

For CS1, only 1-3 SNR observations per satellite were impacted, but these observations showed a significant degradation of 2-3 dB-Hz. This degradation was observed at the exact time of maximum storm intensity over the ETHZ station, which gives a clear indication of the thunderstorm's impact on the observed SNR levels. In comparison to CS1, the SNR degradation observed for CS2 is of a slightly weaker magnitude but more persistent over time, resulting in a much larger number of observations (about 10-20) being affected. This might indicate that the storm system was more stationary for CS2, but radar images suggest that the duration of maximum storm intensity was about 20 minutes for both cases. For both cases, some false detections ahead of the actual event time also suggested a possible earlier impact of the approaching storm systems on specific satellites. However, most of the used satellite tracks crossed the storm track only right around event time, which makes an earlier impact of the thunderstorm unlikely.

The utilized detection algorithm is a very simple statistical approach, which allows for an easy implementation and interpretation of the results. The original algorithm of K. M. Larson (2013), initially developed for the detection of volcanic plumes, was only slightly modified for this study. Our version uses a ten-day average of SNR observations as a background model to calculate SNR residuals and a $2.5 \cdot \sigma_{res}$ detection interval. Nevertheless, the approach also has some limitations such as:

- The sensitivity of GNSS-SNR data is limited (L-band), implying that only severe thunder- and hailstorms could be detected
- GNSS-SNR represents an integral value along the ray path. Therefore, the horizontal resolution is restricted to the satellite tracks.
- Precise (sub-integer level) SNR observations are required, which is limiting the choice of GNSS receivers.
- At this stage, we can neither quantify the contribution of each hydrometeor type (rain vs. hail), nor the influence of the size of the hydrometeors on the magnitude of the degradation
- Other factors potentially contributing to the SNR degradation (such as lightning activity) should be investigated

Future improvements could come from the usage of multi-GNSS and higher-rate observations (e.g. 1 Hz). In this study, we solely used GPS observations, but in recent years, the evolution of multi-GNSS (with the new GNSS systems Galileo and Beidou) has broadened the GNSS signal spectrum significantly. Nowadays a variety of signals on different carrier frequencies are available, which could also be used for approaches like the one presented in this study. An extension to other GNSS is relatively straightforward and planned to be implemented for future investigations. This extension will increase the number of available observations by a factor of two to three and therefore strengthen confidence in the presented approach. Moreover, using 1-Hz observations would increase the amount of data used in this study by a factor of 30. Although already existing GNSS stations might not all record multi-GNSS data at these high frequencies, such considerations should be kept in mind when designing new infrastructure. Furthermore, more sophisticated data mining and machine-learning algorithms might be explored, as their capability to reveal weather phenomena in GNSS products, to which observations should not be directly sensitive, has for example been demonstrated for e.g. downslope wind storms (Aichinger-Rosenberger et al., 2022). Thus, such algorithms might also be capable of separating the signatures of different hydrometeor types (rain and hail) in GNSS data. However, this separation denotes a highly complex task, which most likely will not be possible to achieve using SNR data solely. Therefore, the combination of SNR observations with additional GNSS products also impacted by atmospheric conditions, such as tropospheric signal delays and phase residuals, could be explored. Such approaches will hopefully lead to an improved understanding and identification of all factors accounting for the observed SNR degradation. These factors might include the total amount of water along the ray path (substantial for supercell storms), the ratio of gaseous/liquid/solid particles found in clouds or even lightning events. Measuring the properties of hailstorms is a difficult task due to their rarity and small spatial extent. Hence, being able to use existing and future networks of GNSS stations to detect hailstorms could be very useful. Further investigations comparing storms that produced hail with others that did not could help discriminate a hail signature on GNSS signals.

5 Open Research

The GPS-SNR data sets used in this study are provided at `https://polybox.ethz.ch/index.php/s/mUoWJtyKPZsKs2L`.

Acknowledgments

We thank MeteoSwiss for providing the radar and crowdsourced data and Swisstopo for providing the GNSS data. M.A. acknowledges support from the Swiss Science Foundation project no. CRSII5_201792 J.K. acknowledges support from the Swiss insurance company La Mobilière.

References

Aichinger-Rosenberger, M., Brockmann, E., Crocetti, L., Soja, B., & Moeller, G. (2022). Machine learning-based prediction of alpine foehn events using gnss troposphere products: first results for altdorf, switzerland. *Atmospheric Measurement Techniques*, *15*(19), 5821–5839. Retrieved from `https://amt.copernicus.org/articles/15/5821/2022/` doi: 10.5194/amt-15-5821-2022

Arief, S., & Heki, K. (2020). GNSS Meteorology for Disastrous Rainfalls in 2017–2019 Summer in SW Japan: A New Approach Utilizing Atmospheric Delay Gradients. *Frontiers in Earth Science*, *8*. doi: 10.3389/feart.2020.00182

Asgarimehr, M., Wickert, J., & Reich, S. (2019). Evaluating impact of rain attenuation on space-borne gnss reflectometry wind speeds. *Remote Sensing*, *11*(9). Retrieved from `https://www.mdpi.com/2072-4292/11/9/1048` doi: 10.3390/rs11091048

Asgarimehr, M., Zavorotny, V., Wickert, J., & Reich, S. (2018). Can gnss reflectometry detect precipitation over oceans? *Geophysical Research Letters*, *45*(22), 12,585-12,592. Retrieved from `https://agupubs.onlinelibrary.wiley.com/doi/abs/10.1029/2018GL079708` doi: https://doi.org/10.1029/2018GL079708

Barras, H., Hering, A., Martynov, A., Noti, P.-A., Germann, U., & Martius, O. (2019). Experiences with > 50,000 Crowdsourced Hail Reports in Switzerland. *Bulletin of the American Meteorological Society*, *100*(8), 1429-1440. doi: 10.1175/BAMS-D-18-0090.1

Bevis, M., Businger, S., Herring, T. A., Anthes, R. A., & Ware, R. H. (1992). GPS

Meteorology: Remote Sensing of Atmospheric Water Vapor Using the Global Positioning System. *Geophys. Mag.*, *34*, 359–425.

Brenot, H., Ducrocq, V., Walpersdorf, A., Champollion, C., & Caumont, O. (2006). GPS zenith delay sensitivity evaluated from high-resolution numerical weather prediction simulations of the 8–9 September 2002 flash flood over southeastern France. *Journal of Geophysical Research: Atmospheres*, *111*(D15).

Cegla, A., Rohm, W., Lasota, E., & Biondi, R. (2022). Detecting volcanic plume signatures on gnss signal, based on the 2014 sakurajima eruption. *Advances in Space Research*, *69*(1), 292-307. doi: https://doi.org/10.1016/j.asr.2021.08.034

Douša, J., Dick, G., Kačmařík, M., Brožková, R., Zus, F., Brenot, H., ... Kaplon, J. (2016). Benchmark campaign and case study episode in central Europe for development and assessment of advanced GNSS tropospheric models and products. *Atmospheric Measurement Techniques*, *9*(7), 2989–3008.

Foote, G. B., Krauss, T. W., & Makitov, V. (2005). Hail metrics using conventional radar. *85th AMS Annual Meeting, American Meteorological Society - Combined Preprints*(January), 2791–2796.

Germann, U., Berenguer, M., Sempere-Torres, D., & Zappa, M. (2009). REAL—Ensemble radar precipitation estimation for hydrology in a mountainous region. *Quarterly Journal of the Royal Meteorological Society*, *135*(639), 445–456. doi: 10.1002/qj.375

Germann, U., Boscacci, M., Clementi, L., Gabella, M., Hering, A., Sartori, M., ... Calpini, B. (2022, January). Weather Radar in Complex Orography. *Remote Sensing*, *14*(3), 503. doi: 10.3390/rs14030503

Grapenthin, R., Freymueller, J. T., & Kaufman, A. M. (2013). Geodetic observations during the 2009 eruption of Redoubt Volcano, Alaska. *Journal of Volcanology and Geothermal Research*, *259*, 115-132. (The 2009 Eruption of Redoubt Volcano, Alaska)

Grapenthin, R., Hreinsdóttir, S., & Van Eaton, A. R. (2018). Volcanic Hail Detected With GPS: The 2011 Eruption of Grímsvötn Volcano, Iceland. *Geophysical Research Letters*, *45*(22), 12,236-12,243. doi: https://doi.org/10.1029/2018GL080317

Grapenthin, R., Kyle, P., Aster, R. C., Angarita, M., Wilson, T., & Chaput, J. (2022). Deformation at the open-vent erebus volcano, antarctica, from more than 20 years of gnss observations. *Journal of Volcanology and Geothermal Research*, *432*, 107703. doi: https://doi.org/10.1016/j.jvolgeores.2022.107703

Guerova, G., Jones, J., Dousa, J., Dick, G., Haan, S., Pottiaux, E., ... Bender, M. (2016, 06). Review of the state-of-the-art and future prospects of the ground-based GNSS meteorology in Europe. *Atmospheric Measurement Techniques Discussions*, *9*. doi: 10.5194/amt-9-5385-2016

Gurtner, W., & Estey, L. (2007, December). *Rinex: The receiver independent exchange format version 2.11.* Bern: Astronomical Institute, University of Bern.

Hering, A. M., Morel, C., Galli, G., Senesi, S., Ambrosetti, P., & Boscacci, M. (2004). Nowcasting thunderstorms in the Alpine region using a radar based adaptive thresholding scheme. *Proc. ERAD Confer-ence 2004*, 206-211. Retrieved from `https://www.copernicus.org/erad/2004/online/ERAD04_P_206.pdf`

Hordyniec, P., Kapłon, J., Rohm, W., & Kryza, M. (2018). Residuals of tropospheric delays from gnss data and ray-tracing as a potential indicator of rain and clouds. *Remote Sensing*, *10*(12). doi: 10.3390/rs10121917

Houlié, N., Briole, P., Nercessian, A., & Murakami, M. (2005a). Sounding the plume of the 18 august 2000 eruption of miyakejima volcano (japan) using gps. *Geophysical Research Letters*, *32*(5). doi: https://doi.org/10.1029/2004GL021728

Houlié, N., Briole, P., Nercessian, A., & Murakami, M. (2005b). Volcanic plume above mount st. helens detected with gps. *Eos, Transactions American Geo-*

physical Union, *86*(30), 277-281. doi: https://doi.org/10.1029/2005EO300001
Jones, J., Guerova, G., Dousa, J., Dick, G., Haan, S., Pottiaux, E., ... Pacione, R. (2020). Advanced GNSS Tropospheric Products for Monitoring Severe Weather Events and Climate. In (chap. General Background). Springer.
Kopp, J., Schröer, K., Schwierz, C., Hering, A., Germann, U., & Martius, O. (2022). The summer 2021 switzerland hailstorms: weather situation, major impacts and unique observational data. *Weather*, *n/a*(n/a). doi: https://doi.org/10.1002/wea.4306
Larson, K., Gutmann, E., Zavorotny, V., Braun, J., Williams, M., & Nievinski, F. (2009). Can we measure snow depth with GPS receivers? *Geophysical Research Letters*, *36*(17). doi: https://doi.org/10.1029/2009GL039430
Larson, K., Small, E., Gutmann, E., Bilich, A., Axelrad, P., & Braun, J. (2008, 07). Using GPS multipath to measure soil moisture fluctuations: Initial results. *GPS Solutions*, *12*, 173-177. doi: 10.1007/s10291-007-0076-6
Larson, K. M. (2013). A new way to detect volcanic plumes. *Geophysical Research Letters*, *40*(11), 2657-2660. doi: https://doi.org/10.1002/grl.50556
Lee, S.-W., Yun, S.-H., Kim, D. H., Lee, D., Lee, Y. J., & Schutz, B. E. (2015). Real-time volcano monitoring using GNSS single-frequency receivers. *Journal of Geophysical Research: Solid Earth*, *120*(12), 8551-8569. doi: https://doi.org/10.1002/2014JB011648
MeteoSwiss. (2021a). *Bulletin climatologique juillet 2021.* `https://www.meteosuisse.admin.ch/services-et-publications/publications/rapports-et-bulletins/2021/bulletin-climatologique-juillet-2021.html`. (Accessed 4 May 2023)
MeteoSwiss. (2021b). *Bulletin climatologique juin 2021.* `https://www.meteosuisse.admin.ch/services-et-publications/publications/rapports-et-bulletins/2021/bulletin-climatologique-juin-2021.html`. (Accessed 4 May 2023)
Ridder, N., Ukkola, A., Pitman, A., & Perkins-Kirkpatrick, S. (2022, 12). Increased occurrence of high impact compound events under climate change. *npj Climate and Atmospheric Science*, *5*. doi: 10.1038/s41612-021-00224-4
Roesler, C., & Larson, K. (2018, 06). Software tools for GNSS interferometric reflectometry (GNSS-IR). *GPS Solutions*, *22*. doi: 10.1007/s10291-018-0744-8
Rädler, A., Groenemeijer, P., Faust, E., Sausen, R., & Púčik, T. (2019, 12). Frequency of severe thunderstorms across europe expected to increase in the 21st century due to rising instability. *npj Climate and Atmospheric Science*, *2*, 1-5. doi: 10.1038/s41612-019-0083-7
Shimada, S., Fujinawa, Y., Sekiguchi, S., Ohmi, S., Eguchi, T., & Okada, Y. (1990, 02). Detection of a volcanic fracture opening in Japan using Global Positioning System measurements. *Nature*, *343*. doi: 10.1038/343631a0
Solheim, F. S., Vivekanandan, J., Ware, R. H., & Rocken, C. (1999). Propagation delays induced in gps signals by dry air, water vapor, hydrometeors, and other particulates. *Journal of Geophysical Research: Atmospheres*, *104*(D8), 9663-9670. doi: https://doi.org/10.1029/1999JD900095
Waldvogel, A., Federer, B., & Grimm, P. (1979, December). Criteria for the Detection of Hail Cells. *Journal of Applied Meteorology and Climatology*, *18*(12), 1521–1525. doi: 10.1175/1520-0450(1979)018⟨1521:CFTDOH⟩2.0.CO;2
Wilgan, K., Dick, G., Zus, F., & Wickert, J. (2023, 01). Tropospheric parameters from multi-GNSS and numerical weather models: case study of severe precipitation and flooding in Germany in July 2021. *GPS Solutions*, *27*. doi: 10.1007/s10291-022-01379-0

hailmap_ZRH_20210628.png.

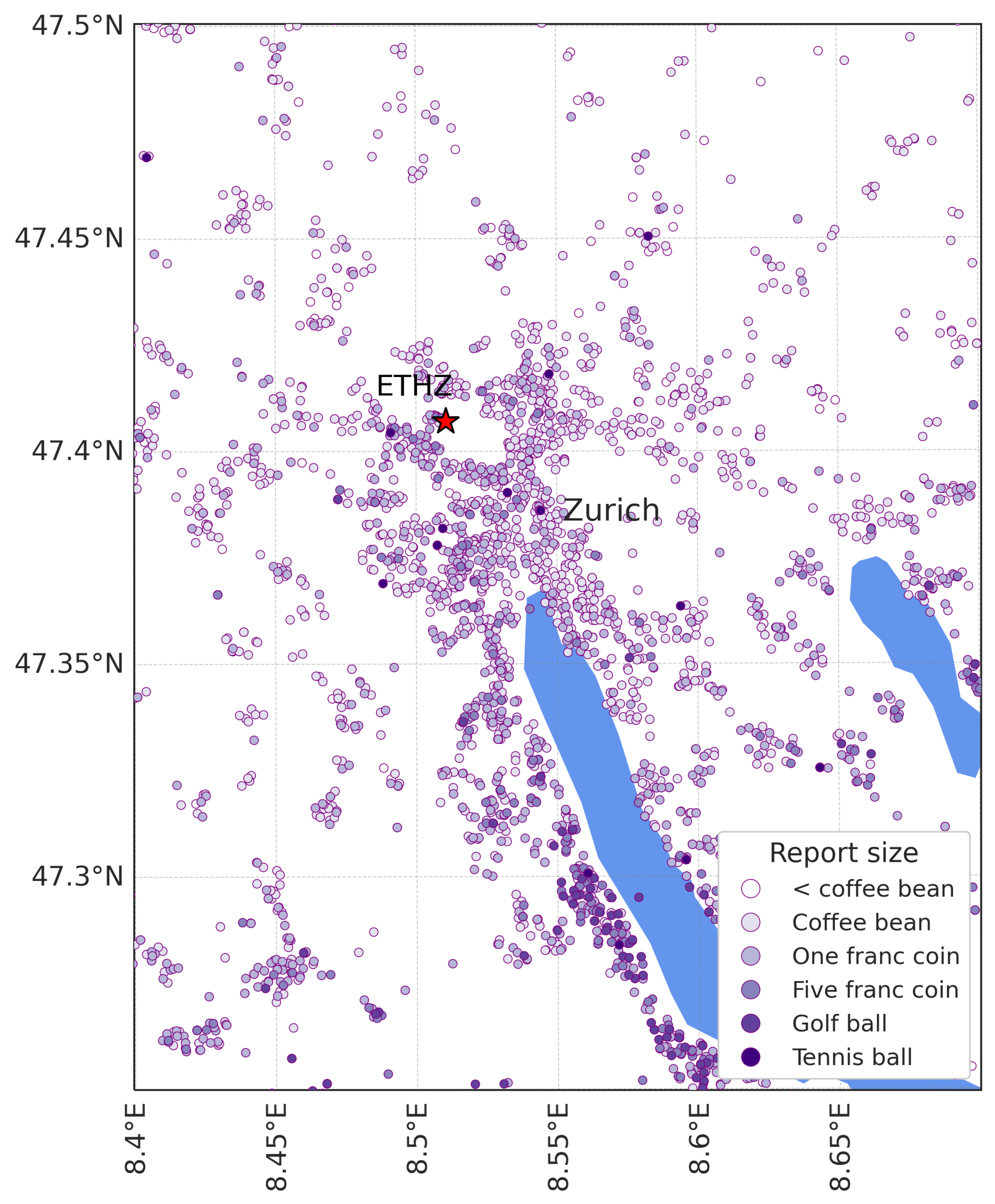
47.5°N
47.45°N
47.4°N
47.35°N
47.3°N
ETHZ
Zurich
Report size
< coffee bean
Coffee bean
One franc coin
Five franc coin
Golf ball
Tennis ball
8.4°E
8.45°E
8.5°E
8.55°E
8.6°E
8.65°E

MaxEcho_ETH_Vertical_10min_20210628.png.

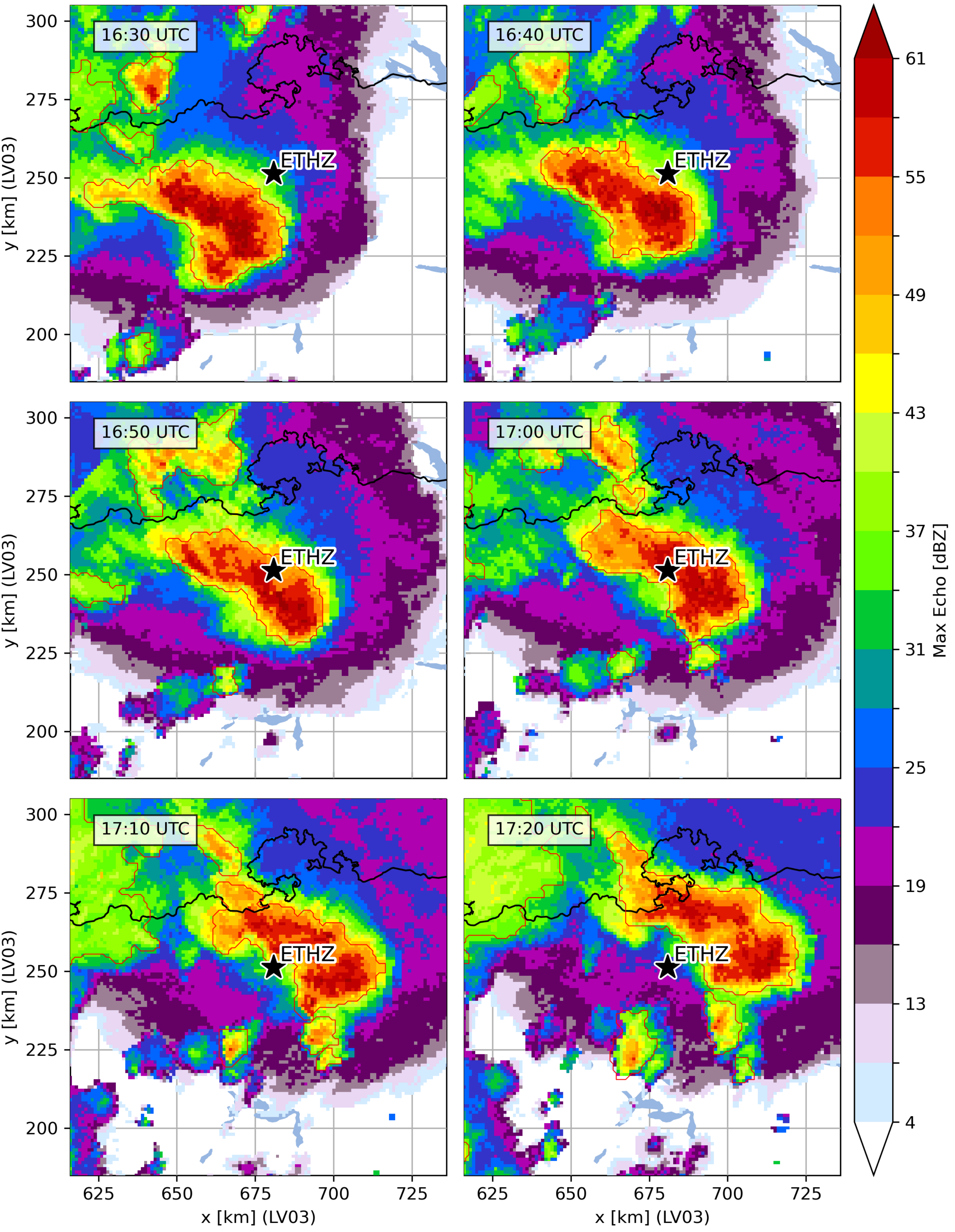

16:30 UTC
16:40 UTC
16:50 UTC
17:00 UTC
17:10 UTC
17:20 UTC
ETHZ
y [km] (LV03)
x [km] (LV03)
300
275
250
225
200
625
650
675
700
725
Max Echo [dBZ]
61
55
49
43
37
31
25
19
13
4

ethz_S2_SNR_residulas_28062021.png.

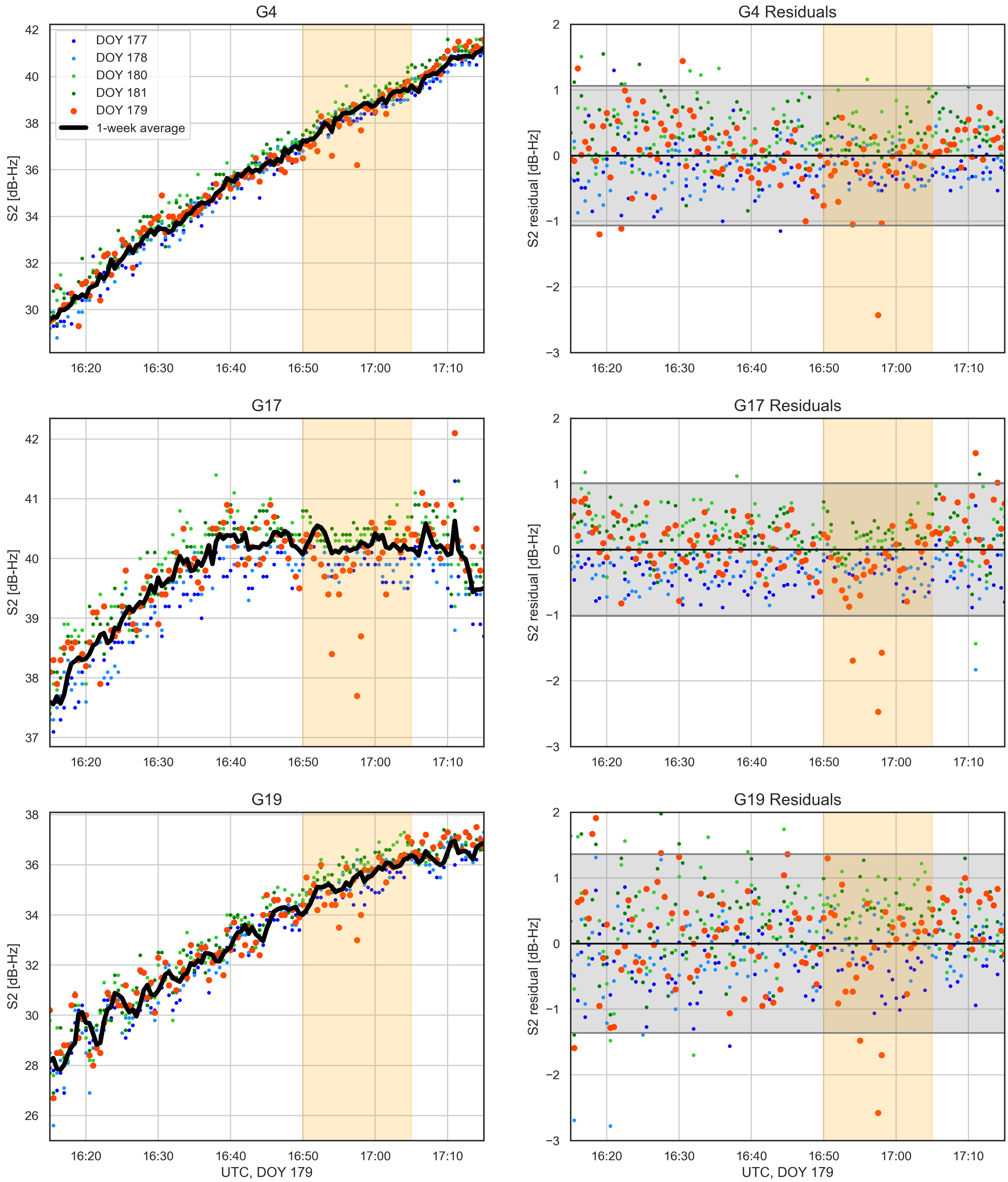

G4
DOY 177
DOY 178
DOY 180
DOY 181
DOY 179
1-week average
S2 [dB-Hz]
G4 Residuals
S2 residual [dB-Hz]
G17
S2 [dB-Hz]
G17 Residuals
S2 residual [dB-Hz]
G19
S2 [dB-Hz]
UTC, DOY 179
G19 Residuals
S2 residual [dB-Hz]
UTC, DOY 179
16:20 16:30 16:40 16:50 17:00 17:10

hailmap_ZRH_20210712.png.

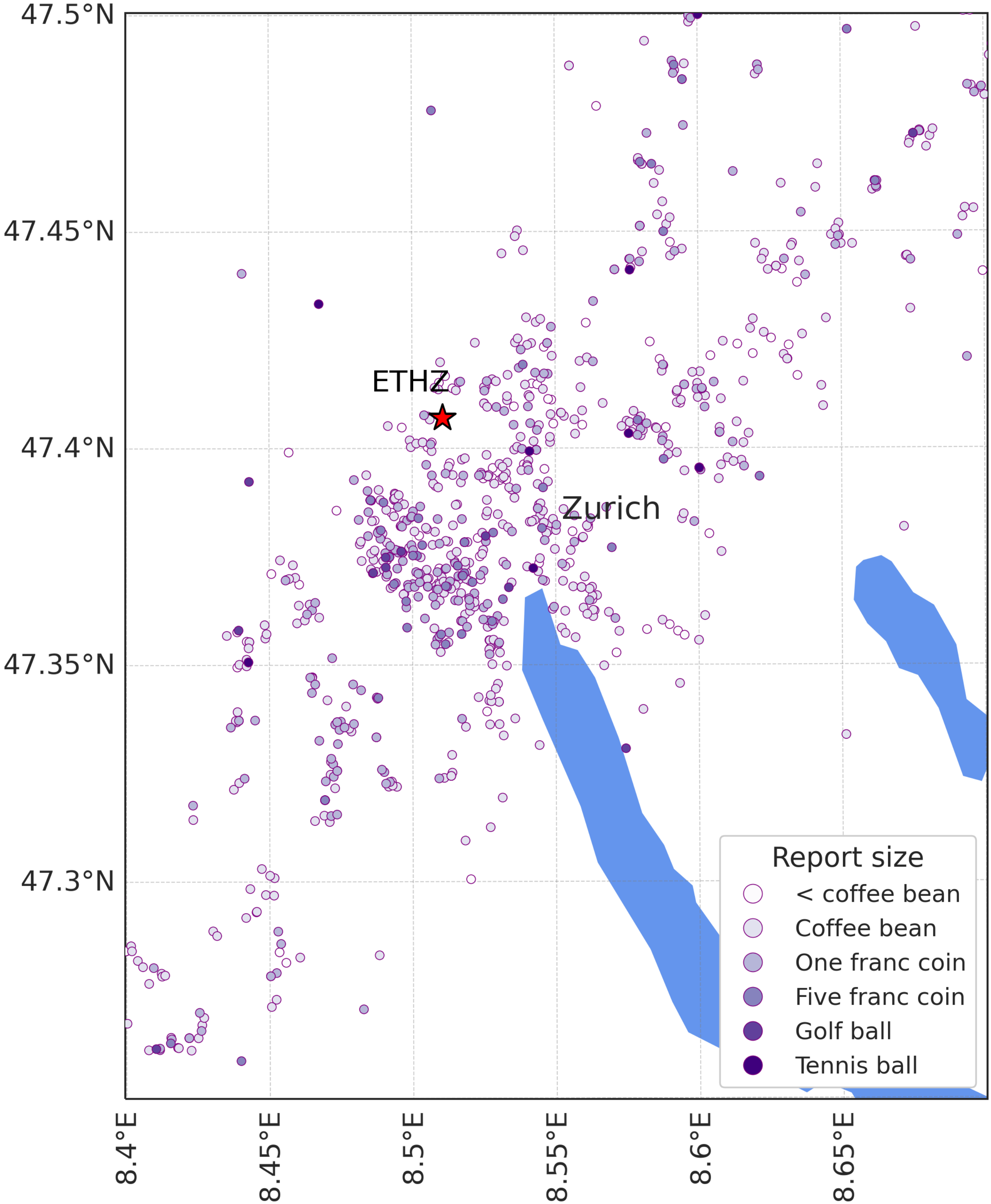
47.5°N
47.45°N
47.4°N
47.35°N
47.3°N
8.4°E
8.45°E
8.5°E
8.55°E
8.6°E
8.65°E
ETHZ
Zurich
Report size
< coffee bean
Coffee bean
One franc coin
Five franc coin
Golf ball
Tennis ball

ethz_S2_SNR_residulas_12072021.png.

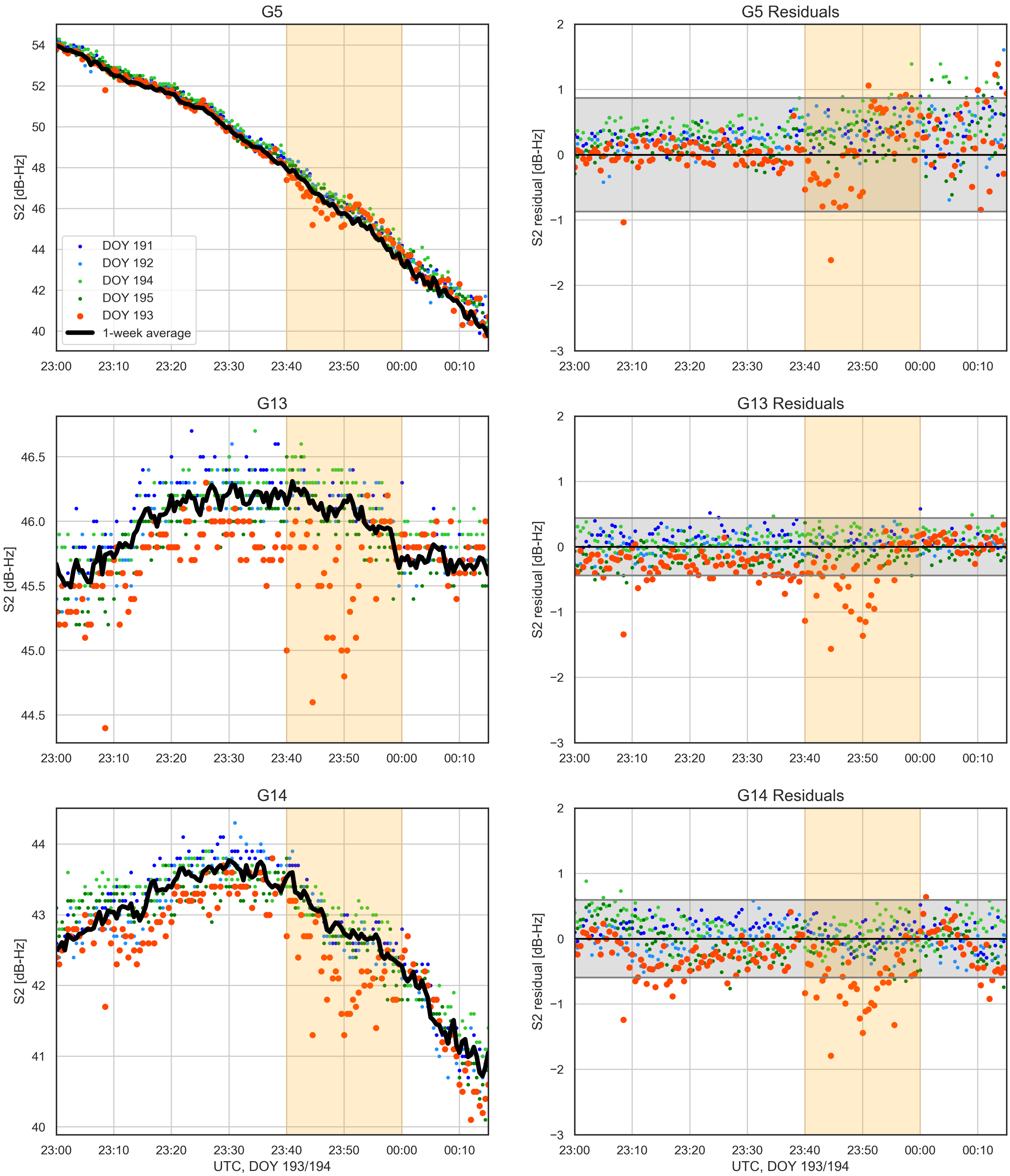

G5
G5 Residuals
G13
G13 Residuals
G14
G14 Residuals
S2 [dB-Hz]
S2 residual [dB-Hz]
DOY 191
DOY 192
DOY 194
DOY 195
DOY 193
1-week average
23:00
23:10
23:20
23:30
23:40
23:50
00:00
00:10
UTC, DOY 193/194

MaxEcho_ETH_Vertical_10min_20210713.png.

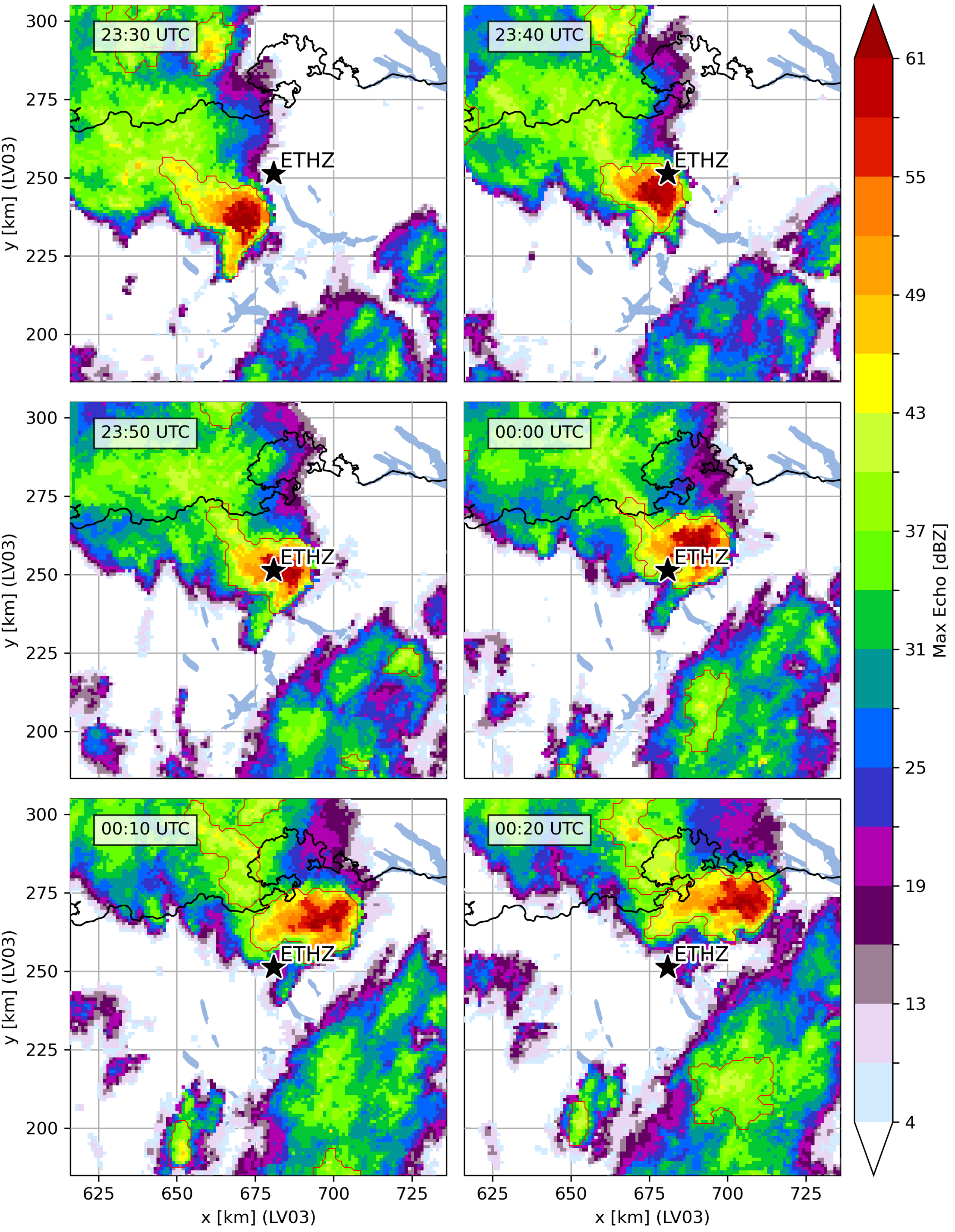
23:30 UTC
23:40 UTC
23:50 UTC
00:00 UTC
00:10 UTC
00:20 UTC
ETHZ
y [km] (LV03)
x [km] (LV03)
Max Echo [dBZ]
300
275
250
225
200
625
650
675
700
725
4
13
19
25
31
37
43
49
55
61